Supporting Information for:

Synergizing between interband/intraband defect states in prolonging charge carrier lifetime of InSe/SiH heterojunction

Qi Zhao, Jinlu He*

College of Chemistry and Chemical Engineering, Inner Mongolia University, Hohhot 010021, PR China

Theoretical methodology

In order to investigate the effects of inter and intraband defects on the charge transfer and recombination processes in semiconductor heterojunctions, we constructed a periodically repeated InSe/SiH heterojunction using the 64-atom InSe (4 ×4) (001) surface and 64-atom SiH (4 ×4) (001) surface. The optimized lattice constants of optimized InSe and SiH supercell are 16.00 Å and 15.32 Å, respectively, along *a* and *b* directions, resulting in only a 0.68 Å lattice mismatch between the two slabs. A 15 Å vacuum was added normal to the surface to eliminate the interaction between the periodic images. We considered four types of vacancy defects in InSe/SiH heterojunction, including indium (V_{In}), selenium (V_{Se}), silicon (V_{Si}), and hydrogen (V_H) vacancies. The InSe/SiH heterojunctions with vacancies were built by removing one

* Corresponding author, E-mail: hejinlu@imu.edu.cn

corresponding atom at the interface. The formation energies (E_f) were calculated using the formula: $E_f = E_{defect} - E_{pristine} + \mu(X)$. Here, E_{defect} and $E_{pristine}$ are total energy of the defective and pristine systems. $\mu(X)$ is the chemical potential of In, Se, Si or H atom.

All DFT calculations, including geometric optimization, electronic structure, adiabatic MD, and NA coupling calculations, were carried out using Vienna ab initio Simulation Package (VASP).[1] The exchange−correlation interactions were treated with the Perdew-Burke-Ernzerhof (PBE) functional,[2] while the interactions between the valence electrons and ionic cores were described using the projector augmented wave (PAW) method.[3] The van der Waals (vdW) interactions were accounted for using the Grimme DFT-D3 approach.[4] The plane-wave basis energy cutoff was set at 400 eV. A 2 × 2 × 1 Γ-centered Monkhorst-Pack k-point mesh was utilized for the geometric optimization. To obtain an accurate electronic structure, a denser 8×8×1 k-point mesh was employed.[5]

During the NAMD simulations, we treated the heavier nuclei and lighter electrons with (semi)classically and quantum mechanics. After geometry optimization, three heterojunctions were heated to 300 K by velocity rescaling. Then, 6 ps MD trajectories were generated with a 1 fs time step. and 1000 geometries were selected as initial conditions for the NAMD simulations. We carried out the simulation of electron transfer using the fewest switching surface hopping (FSSH)[6, 7], and the hole transfer and charge recombination were calculated with the decoherence induced surface hopping (DISH)[8]. The PYXAID code was utilized to carry out the NAMD simulations

for the charge carrier dynamics.[9, 10] For each initial condition, 2000 stochastic processes were sampled for the NAMD simulations.

NA-MD in the Basis of Kohn-Sham (KS) Orbitals

The standard time-dependent density functional theory (TDDFT) utilizes the electron density to characterize the electronic properties of the system,[11] and the electron density $\rho(\boldsymbol{r},t)$ is equivalent to the sum of the densities of the KS orbital, $\Phi_p(\boldsymbol{r},t)$, each occupied by a single electron.

$$\rho(\boldsymbol{r},t) = \sum_{p=1}^{N_e} \left|\Phi_p(\boldsymbol{r},t)\right|^2 \quad (1)$$

The evolution of the electron density is treated by the TD variational principle to create the single-electron equations for the evolution of the KS orbitals:[12, 13]

$$i\hbar \frac{\partial \Phi_p(\boldsymbol{r},t)}{\partial t} = H(\boldsymbol{r},\boldsymbol{R},t)\Phi_p(\boldsymbol{r},t);\ p=1,\ 2,\ \ldots,\ N_e \quad (2)$$

These equations are nonlinear because the Hamiltonian H(r, R, t) is a functional of the electron density. To obtain the nuclear configuration, the time-dependent KS orbitals are expanded in the adiabatic KS orbital basis, $\widetilde{\Phi}_k\big(\boldsymbol{r};\boldsymbol{R}(t)\big)$.

$$\Phi_p(\boldsymbol{r},t) = \sum_{k=0}^{N} c_k(t)\widetilde{\Phi}_k(\boldsymbol{r};\boldsymbol{R}(t)) \quad (3)$$

The lower and upper bounds for the sum in Eq. (3) is zero and the size of the electronic basis set used in temporal evolution. The expansion coefficients are obtained by inserting eq 3 into eq 2:[14]

$$i\hbar \frac{\partial}{\partial t} c_m(t) = \sum_{k=1}^{N_e} c_k(t)(\varepsilon_k \delta_{km} + \boldsymbol{d}_{km} \cdot \dot{\boldsymbol{R}}) \quad (4)$$

Here, ε_k represents the energy of the adiabatic state m, and δ_{km} denotes nonadiabatic (NA) coupling between states *k* and *m*. The value of NA coupling is related to the strength of electron-phonon interaction, and its value can be obtained through the

numerical calculation method expressed in the following equation:[15]

$$\boldsymbol{d}_{km} \cdot \dot{\boldsymbol{R}} = -i\hbar\langle\widetilde{\Phi}_k|\nabla_R|\widetilde{\Phi}_m\rangle \cdot \frac{d\boldsymbol{R}}{dt} = -i\hbar\left\langle\widetilde{\Phi}_k\middle|\frac{\partial}{\partial t}\middle|\widetilde{\Phi}_m\right\rangle$$

$$\approx -\frac{i\hbar}{2\Delta t}\left(\langle\widetilde{\Phi}_k(t)|\widetilde{\Phi}_m(t+\Delta t)\rangle - \langle\widetilde{\Phi}_k(t+\Delta t)|\widetilde{\Phi}_m(t)\rangle\right) \quad (5)$$

In mixed quantum-classical dynamics methods, such as the Ehrenfest and surface hopping methods, the nuclei and electrons are coupled to each other, and their motions affect each other. Condensed matter systems generally contain a large number of nuclei and electrons. Considering the feedback effect of electrons in quantum systems on atomic nuclei in classical systems, the calculation amount required is very large, which limits the application of such methods in condensed matter systems. Based on the fact that the effect of electron excitation on the motion of the nucleus in a large condensed matter system is negligible compared to the effect of thermal effects, Prof. Prezhdo proposed the hypothesis of Classical Path Approximation (CPA).[14] This hypothesis states that the motion of the nucleus is not affected by the motion of the electron, and the time-dependent evolution of the electron is still influenced by the motion of the nucleus. Therefore, the NAMD process can be calculated by using the trajectory of nuclear time-dependent evolution in the ground state instead of the trajectory in the excited state. After a transition between electronic states occurs in Tully's FSSH method, velocity rescaling and jump inhibition provide a careful balance between upward and downward transitions of energy, resulting in Boltzmann statistics and quantum-classical thermodynamic equilibria. For the probability of the fewest surface transitions, Prof. Prezhdo' group instead uses multiplication by Boltzmann's constant. In this approximation, it is not necessary to readjust the velocity of the nucleus along the

determined NA coupling direction after the transition occurs, and the calculation amount is greatly reduced.

In general, the FSSH assigns a probability for transitioning from the current electronic state *j* to the new state *k* during a sufficiently small time interval Δt, as follows:

$$P_{j\to k}^{*} = \int_{t}^{t+dt} \frac{2}{C_j^{*}(t)c_k^{*}(k)} Re\left[\left(\frac{jH_{jk}}{\hbar}\right) C_j^{*}(t)c_k^{*}(k)\right] dt \tag{6}$$

$$F_{j\to k} = P_{j\to k}^{*} B_{j\to k} \tag{7}$$

$$B_{j\to k} = \begin{cases} \exp\left(-\frac{E_j - E_k}{k_B T}\right), E_j > E_k \\ 1\ , \quad E_j \le E_k \end{cases} \tag{8}$$

To reflect the detailed balance condition, the standard FSSH's transition probabilities, $P_{j\to k}^{*}$, are replaced, $F_{j\to k}$, with in the Prof. Prezhdo' FSSH by scaling the transition probabilities with the Boltzmann factor, $B_{j\to k}$. The E_j and E_k are the energy of electronic state *j* and *k*.

Although the simplified FSSH method can describe the NAMD of some systems, it has an important flaw: it ignores the decoherence problem. Because each quantum state in a quantum system is inherently coherent, it will maintain its original coherence unless interfered with by the external environment. When the system is interfered with by the outside world and becomes entangled among states, the system will soon collapse into a particular quantum state. This process is commonly referred to as quantum decoherence. Since nuclear wave packets do not exist in quantum-classical simulations, the quantum decoherence effect must be introduced as a semiclassical correction. Fast decoherence causes the electron wave function to collapse onto a simple quantum state, generally slowing down quantum dynamics. In order to address the decoherence loss problem in the fewest-switches surface hopping (FSSH) method,

Prof. Prezhdo proposed two nonadiabatic dynamics methods that take the quantum decoherence effect into account: namely, decoherence-induced surface hopping (DISH))[8] and decoherence-corrected surface hopping (DCSH)[16, 17] methods. The DISH method is briefly introduced below.

The DISH method is based on the physical process wherein decoherence serves as the basis for evolutionary branching in quantum mechanics.[18-20] It simultaneously incorporates decoherence into quantum-classical NAMD and utilizes decoherence as the source of classical trajectory branching, where surface jumps occur precisely at decoherence events. During decoherence time, all other quantum states collapse to quantum state i.

$$t_i(\mathrm{t}) > \tau_i(t) \tag{9}$$

In the above equation, t is the physical time, t_i is the time when the last decoherence event occurs, and $\tau_i(t)$ is the decoherence time of the quantum state i. $\tau_i(t)$ is defined as follows:

$$\frac{1}{\tau_i(t)} = \sum_{j=1, j\neq i}^{N} \left|c_j(t)\right|^2 r_{ij} \tag{10}$$

r_{ij} in equation (9) represents the decoherence rate between electronic states i and j, and is the reciprocal of the decoherence time. The coefficient $c_j(t)$ is obtained by solving the time-dependent Schrodinger equation in equation (8). When a decoherence event occurs, a random number ζ is generated. When $|\left|c_j(t)\right|^2 > \zeta$, the trajectory transitions to the electron state i, otherwise $c_j(t) = 0$ is set, the electron state i is projected, and the remaining wave function is normalized again.

Decoherence time is calculated using pure dephasing time in optical response

theory. The Autocorrelation Function (ACF) of the energy gap fluctuation between phonon-induced electron state and hole state is expressed by the following formula:

$$C(t) = \langle \Delta E(t) \Delta E(0) \rangle_T \tag{11}$$

Angle brackets in the above formula represent the average value, and the ACF adopts the following formula for normalization:

$$C_{norm}(t) = \frac{\langle \Delta E(t) \Delta E(0) \rangle_T}{\langle \Delta E(0)^2 \rangle_T} \tag{12}$$

In equation (11), $\Delta E(0)^2$ represents the initial value, and the square root of $C_{norm}(t)$ gives the average fluctuation of the excitation energy. A second-order cumulative expansion of the optical response function is used to calculate the pure dephasing function.[21]

$$D_{cumu}(t) = \exp(-g(t)) \tag{13}$$

$$g(t) = \int_0^t d\tau_1 \int_0^{\tau_1} d\tau_2 \, C(\tau_2) \tag{14}$$

The Gaussian function is used to fit equation (2-36), and the pure dephasing time is obtained. The shorter the time, the faster the electron wave function collapses to the pure electron state, and this generally slows down quantum dynamics. Fourier transform is used to obtain the energy spectral density of the ACF:

$$I(\omega) = \left| \frac{1}{\sqrt{2}} \int_{-\infty}^{\infty} dt e^{-i\omega t} C(t) \right|^2 \tag{15}$$

Table S1. Averaged Carrier-phonon Nonadiabatic Couplings (meV) between States (*i* and *j*) in the Pristine InSe/SiH and V_{Se} Systems.

	Pristine	V_{Se}
CBM+1/CBM	8.55	12.66
CBM+2/CBM	6.73	7.33
CBM+3/CBM	5.58	6.13
CBM+4/CBM	4.95	6.10
CBM+5/CBM	4.12	5.76
CBM+6/CBM	3.66	5.44
CBM+7/CBM	2.46	3.64
CBM+8/CBM	1.78	3.77
CBM+9/CBM	2.10	3.11
CBM+10/CBM	2.22	2.66
CBM+11/CBM	1.88	2.79
CBM+12/CBM	1.83	
CBM+13/CBM	1.80	
CBM+1/CBM+2	11.62	9.72
CBM+2/CBM+3	11.09	12.10
CBM+3/CBM+4	13.53	13.41
CBM+4/CBM+5	12.47	10.66
CBM+5/CBM+6	10.08	9.32

CBM+6/CBM+7	7.53	8.03
CBM+7/CBM+8	12.08	12.55
CBM+8/CBM+9	19.07	18.74
CBM+9/CBM+10	20.91	29.58
CBM+10/CBM+11	25.16	33.62
CBM+11/CBM+12	26.38	
CBM+12CBM+13	32.86	
VBM-1/VBM	0.34	1.55
VBM-2/VBM	0.32	0.72
VBM-1/VBM-2	14.16	17.19

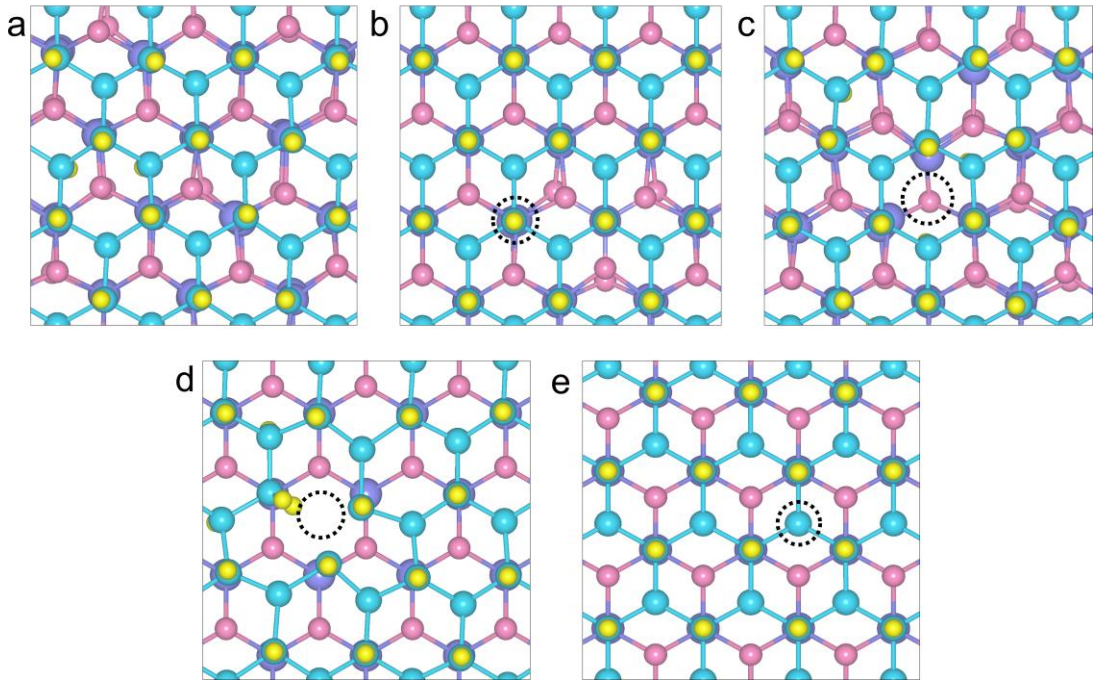

Fig. S1. Top views of InSe/SiH heterojunctions with or without vacancy. (a) pristine, (b)V_{In}, (c)V_{Se}, (d)V_{Si}, and (e)V_{H} systems. The dashed circles denote vacancy regions, and the purple, pink, cyan and yellow balls represent In, Se, Si and H atoms, respectively.

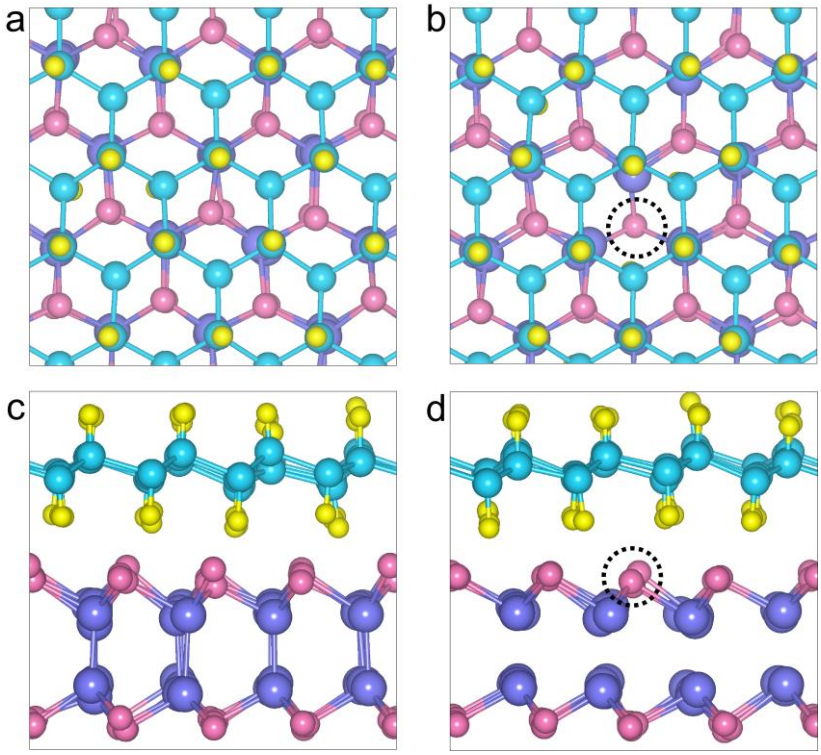

Fig. S2. Top and side views of InSe/SiH heterojunctions with or without vacancy at 300 K. (a, c) pristine InSe/SiH heterojunction, (b, d) V_{Se} systems. The dashed circles denote vacancy regions, and the purple, pink, cyan and yellow balls represent In, Se, Si and H atoms, respectively.

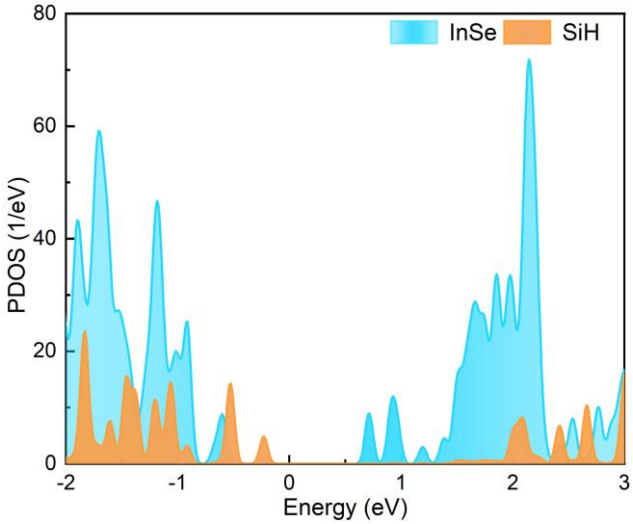

Fig. S3. The projected densities of states (PDOS) of InSe/SiH heterojunction with Se vacancy located outside the two layers calculated using the PBE functional. The Fermi energy is set to zero.

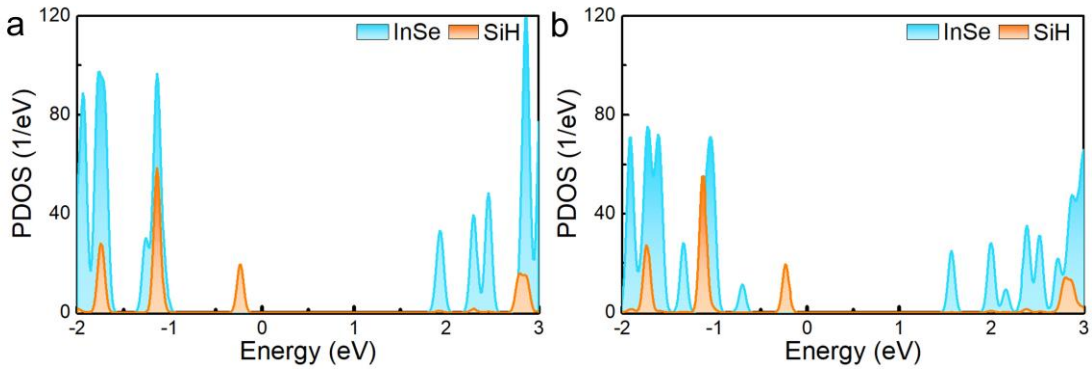

Fig. S4. The projected densities of states (PDOS) of (a) pristine and (b) V_{Se} systems calculated using the HSE06 functional. The Fermi energy is set to zero.

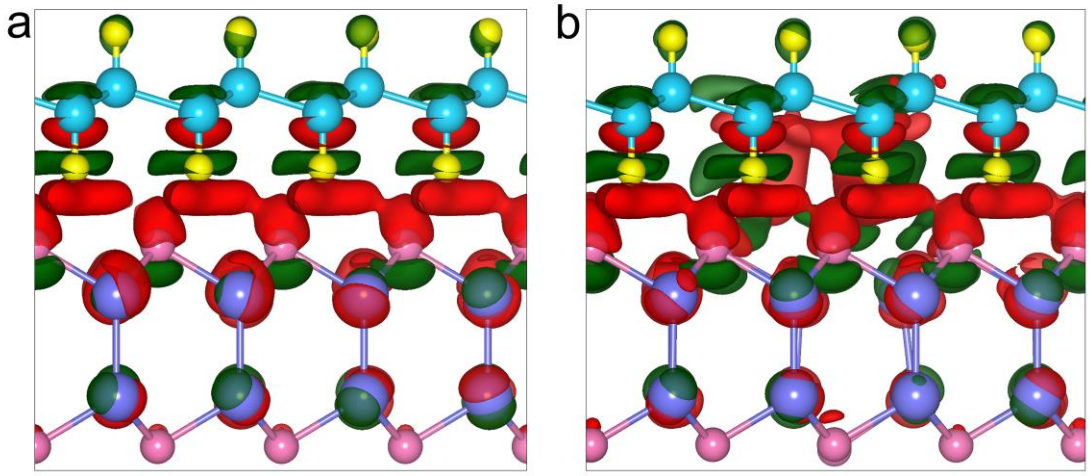

Fig. S5. Differential charge densities of InSe/SiH with or without vacancy defect. (a) pristine InSe/SiH heterojunction, (b) V_{Se} systems. The red and green regions represent charge accumulation and depletion. The isosurface values are set to 0.0001 eV/Å^3.

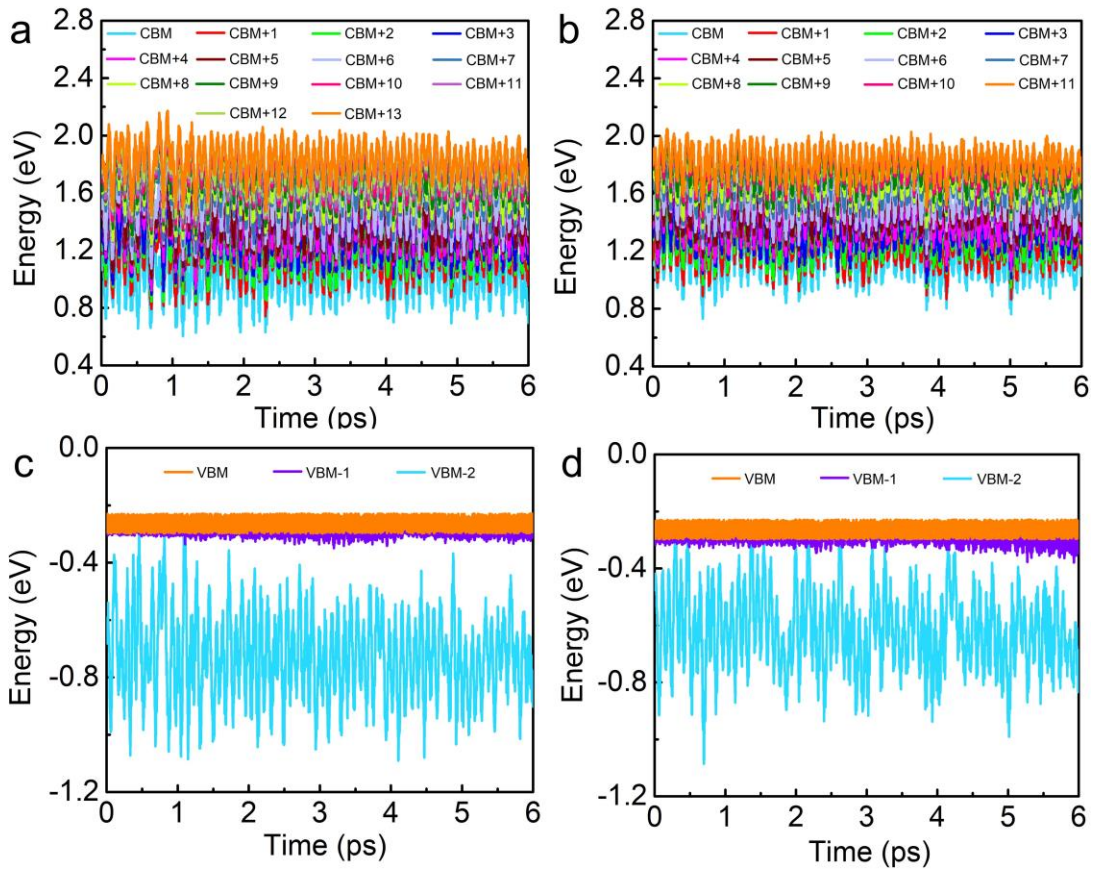

Fig. S6. Time-dependent KS orbitals energies for the electron and hole transfer processes. (a) electron, (c) hole transfer for pristine system; (b) electron, (d) hole transfer for V_{Se} system.

References

1 G. Kresse and J. Furthmüller, *Phys. Rev. B: Condens. Matter Mater. Phys.*, 1996, **54**, 11169-11186.

2 J. P. Perdew, K. Burke and M. Ernzerhof, *Phys. Rev. Lett.*, 1996, **77**, 3865-3868.

3 P. E. Blöchl, *Phys. Rev. B: Condens. Matter Mater. Phys.*, 1994, **50**, 17953−17979.

4 S. Grimme, J. Antony, S. Ehrlich and H. Krieg, *J. Chem. Phys.*, 2010, **132**, 154104.

5 H. J. Monkhorst and J. D. Pack, *Phys. Rev. B*, 1976, **13**, 5188-5192.

6 C. F. Craig, W. R. Duncan and O. V. Prezhdo, *Phys. Rev. Lett.*, 2005, **95**, 163001.

7 Tully and C. John, *J. Chem. Phys.*, 1990, **93**, 1061-1071.

8 H. M. Jaeger, S. Fischer and O. V. Prezhdo, *J. Chem. Phys.*, 2012, **137**, 22A545.

9 A. V. Akimov and O. V. Prezhdo, *J. Chem. Theory Comput.*, 2013, **9**, 4959.

10 A. V. Akimov and O. V. Prezhdo, *J. Chem. Theory Comput.*, 2014, **10**, 789.

11 M. Petersilka, U. Gossmann and E. Gross, *Phys. Rev. Lett.*, 1996, **76**, 1212-1215.

12 W. Kohn and L. J. Sham, *Phys. Rev.*, 1965, **140**, A1133-A1138.

13 C. M. Isborn, X. Li and J. C. Tully, *J. Chem. Phys.*, 2007, **126**, 134307.

14 C. F. Craig, W. R. Duncan and O. V. Prezhdo, *Phys. Rev. Lett.*, 2005, **95**, 163001.

15 S. Hammes-Schiffer and J. C. Tully, *J. Chem. Phys.*, 1994, **101**, 4657-4667.

16 B. J. Schwartz, E. R. Bittner, O. V. Prezhdo and P. J. Rossky, *J. Chem. Phys.*, 1996, **104**, 5942-5955.

17 B. F. Habenicht and O. V. Prezhdo, *Phys. Rev. Lett.*, 2008, **100**, 197402.

18 O. V. Prezhdo, *J. Chem. Phys.*, 1999, **111**, 8366-8377.

19 I. C. Percival, *Proc. Roy. Soc. A*, 1994, **447**, 189-209.

20 G. Milburn, *Phys. Rev. A*, 1991, **44**, 5401.

21 S. Mukamel, *Principles of nonlinear optical spectroscopy*, Oxford University Press, New York, 1995.